PALEO-EXTENT OF MARS' MASSIVE CO2 ICE DEPOSIT. P.B. Buhler. Planetary Science Institute (pbuhler@psi.edu)

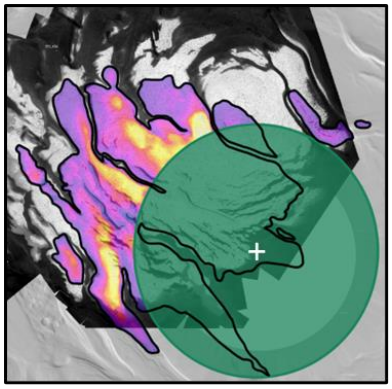

Fig. 1. Present-day CO_2 Deposit extent (black outline) [1]. Cross = pole. 0° E is up, 90° E right. Colorized region indicates radar-derived present-day CO_2 Deposit thickness [2] overlaid on MOLA hillshade [3] and CTX mosaic [4]. Colors indicate thickness: 0 m (purple) to 946 m (orange). Poleward of 87° S no radar observations are available (green circle).

Introduction: Mars' present-day South Polar Massive CO_2 Ice Deposit ("CO_2 Deposit") has a mass comparable to Mars' present-day, primarily CO_2, atmosphere [1-2,5-6]. The CO_2 Deposit exchanges with the atmosphere and CO_2 adsorbed in the regolith on ~100 kyr timescales in response to cyclic variations in Mars' latitudinal sunlight distribution, driven by orbital obliquity variations [1,7-8]. Recent work proposed that the CO_2 available to exchange between the CO_2 Deposit, atmosphere, and regolith on 100-kyr timescales is 5-50× larger than Mars' current atmospheric mass (with CO_2 presently held mainly in the regolith) [8]. The prediction implies that during recent (<1 Myr ago) obliquity minima (~15°), polar CO_2 ice deposition (sourced mainly from regolith CO_2 desorption) would create a paleo-CO_2 Deposit 5-50× more massive than the present-day (obliquity = ~25°) CO_2 Deposit.

Such a large flux of CO_2 not only has critical implications for many aspects of Mars' climate – especially the availability of conditions necessary to sustain near-surface liquid water during the Noachian (e.g., [9-11]), Hesperian (e.g. [12]), and Amazonian (e.g., [8]) – but also for the interpretation of the historical climate record stored in Mars' south polar deposits [13-14]. For example, this large transport of CO_2 has important implications (~2×) for the average pressure of Mars throughout the Amazonian, depending on the mass of CO_2 exchanging between these reservoirs [8]. Because the pressure-temperature phase space of Mars' atmosphere is near the stability point for near-surface liquid water, determining Mars' historical atmospheric pressure history is a critical step for determining not only the basic characteristics of its atmospheric workings, but also the recent availability of near-surface liquid water for bio/geo/chemical processes. Moreover, tracking the obliquity-driven flux of CO_2 is essential for determining Mars' regolith CO_2 adsorption capacity, which is important for elucidating the availability of CO_2 to drive climatic processes [e.g., 15], especially those proposed to sustain Noachian near-surface liquid water (e.g., [9-11,16]).

This abstract reports an initial survey to identify (i) features associated with the degradation of the current CO_2 Deposit and (ii) distribution of similar features located outside the perimeter of the present-day CO_2 Deposit (likely remnants of a paleo-CO_2 Deposit).

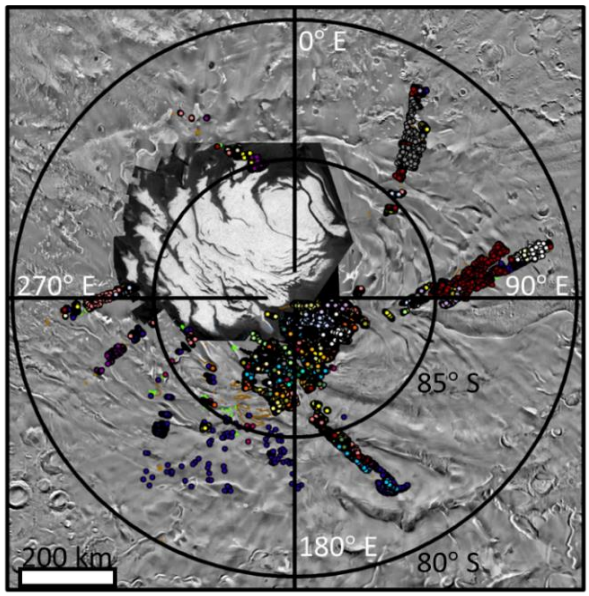

Fig. 2. Over 10,000 morphologic features associated with a paleo-CO_2 Deposit were identified covering a ~3×10^4 km^2 region near 90-215° E, poleward of ~86° and along transects extending to ~81° S at longitudes ~30, 90, 150, 210, 270, and 330°. Paleo-CO_2-Deposit-related morphologies extend 100s of km beyond the dense pilot mapping region. Colored dots correspond to morphologic feature color keys in Fig. 3.

Methods: Mapping was performed using ~100 Context Camera (CTX) [17] and High Resolution Imaging Science Experiment (HiRISE) [18] images. Mapping focused on a near-polar region {~90—225° E, ~87—90° S} and along transects from the pole to 75° S at 60°-longitude increments to assess the equatorward extent of features associated with a paleo-CO_2 Deposit (Fig. 2). Features were assessed and categorized using a variety of morphological characteristics, including scale, spacing, relief, angularity, and shape.

Results: Mapping identified deflationary features on the present-day CO_2 Deposit and ~10,000 similar features beyond the extent of the present-day CO_2 Deposit, to ~81° S (Figs. 2,3). Mapping also identified contacts where the edge of the present-day CO_2 Deposit onlaps onto older, underlying South Polar Layered Deposit (SPLD) outcrops and analogous contacts between paleo-CO_2-Deposit morphology and the SPLD, as well as deflationary morphology similar to that of

the present-day CO_2 Deposit, but 100s of km beyond the extent of the present-day CO_2 Deposit, contiguously draping underlying Layered Deposit terrain.

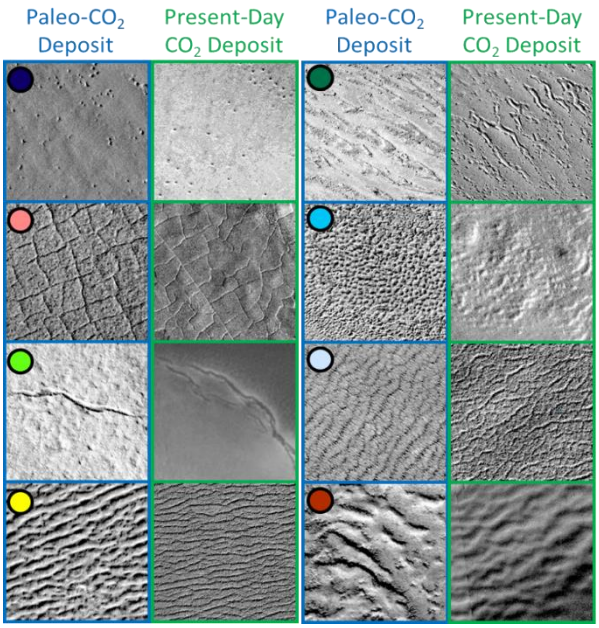

Fig. 3. Eight selected morphologies identified during mapping outside the current boundary of the CO_2 Deposit (blue columns) analogous to present-day CO_2 Deposit terrain (green columns), including pitted, polygonal, fractured, rippled, fluted, stippled, wrinkled, and hummocked terrains. In total, more than 20 analogous terrain types have been identified. Each panel shows a CTX image portion 1 km across. Colored dots correspond to map color labels (Fig. 2).

Discussion: A compelling and widespread suite of morphologic features and geologic associations preserving the remnants of paleo-CO_2 Deposits from prior CO_2 glacial cycles extending from the pole to ~81° S have been identified. These features are interpreted as paleo-CO_2 Deposit markers because they (1) have morphology and associations similar to present-day CO_2 Deposit features, (2) are in close proximity to the present-day Deposit (range-restricted, poleward of ~81° S), (3) are generally within the extent of model-predicted paleo-CO_2 Deposits [e.g., 8,19], and (4) are dissimilar to features found elsewhere on Mars, when considered in detail.

Paleo-CO_2 Deposit terrains likely arise from the sublimation of CO_2 from beneath dusty H_2O lag layers that develop during the obliquity-driven deposition-ablation cycle of the CO_2 Deposit (Fig. 4). The CO_2 Deposit formed through exchange between polar CO_2 ice, atmospheric CO_2, and CO_2 adsorbed in regolith, driven by Mars' cyclic obliquity evolution over the past 510 kyr [8]. When obliquity decreases, polar sunlight decreases, and the MCID accumulates CO_2 ice (with H_2O ice and dust impurities). When obliquity increases, CO_2 ablates, leaving behind lag layers (i.e., BLs) of residual H_2O ice and dust.

Presently, the CO_2 Deposit is ablating [8], so H_2O ice lag overlies a main subliming CO_2 ice body. As CO_2 sublimes and escapes through overlying H_2O ice, the CO_2 deposit deflates, which morphologically manifests as the formation of pits, fractures, polygons, etc. in the dusty H_2O ice lag (Fig. 2; [5,7,20]). Likewise, dusty H_2O ice lag layers formed during previous CO_2 glacial ablation cycles [1-2,21]. Dusty H_2O ice layers are ~10s-of-meters thick [1-2,21] and are much less volatile than CO_2 ice and so mark the former extent of the paleo-CO_2 Deposit long after the CO_2 ice is gone.

Planned future work includes additional mapping, morphologic analysis, and comparison of the observed extent of the paleo-CO_2 Deposit to predicted extents from physics-based modeling in order to better quantify Mars' global exchangeable CO_2 inventory. The paleo-CO_2 Deposit features identified here have not been previously described or mapped, making their identification and analysis an essential part of quantitatively investigating Mars' global CO_2 inventory.

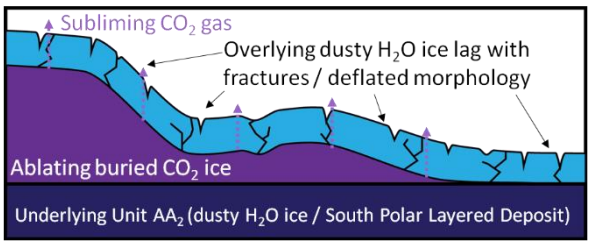

Fig. 4. Schematic deflationary morphology formation within the overlying dusty H_2O ice lag deposit. Note, at right side of panel, the CO_2 Deposit has completely ablated, leaving behind the dusty H_2O ice lag unconformably overlaying the older basement ice. The dusty H_2O lag persists long after the underlying CO_2 has sublimed, imprinted with the deflationary morphologic signature of underlying CO_2 ice sublimation.

Acknowledgments: Work supported by NASA Grant 80NSSC21K1088. **References:** [1] Bierson, C. et al., 2016. *GRL* 43, 4172–4179. [2] Alwarda, R., Smith, I.B., 2021. *JGR Plan.* e2020JE006767. [3] Smith, D. et al., 2001. *JGR Plan.* 106, 23689. [4] Thomas, P. et al., 2016. *Icarus* 268, 118. [5] Phillips, R. et al., 2011. *Science* 332, 838. [6] Putzig, N. et al., 2018. *Icarus* 308, 138. [7] Buhler, P. et al., 2020. *Nat. Astro.* 4, 364-371. [8] Buhler, P. & Piqueux, S., 2021. *JGR Plan.* 126, e2020JE006759. [9] Forget, F. et al., 2013. *Icarus* 222, 81. [10] Wordsworth, R. et al., 2015. *JGR Plan.* 120, 1201. [11] Buhler, P., 2022. doi: 10.21203/rs.3.rs-1287989/v1 [12] Kite, E. et al., 2017. *GRL* 44, 3991. [13] Smith, I. et al., 2020. *PSS* 184, 104841. [14] Becerra, P. et al., 2021. *PSJ* 2, 209. [15] Jakosky, B., 2021. *Ann Rev EPS* 49, 71 [16] Fassett, C. & Head, J., 2011. *Icarus* 211, 1204. [17] Malin, M. et al., 2007. *JGR Plan*, 112, E05S04. [18] McEwen, A. et al., 2007. *JGR Plan* 112(E5). [19] Fanale, F. et al., 1982. I*carus* 50, 381. [20] Buhler, P. & Smith, I., 2022. LPSC 53, #2678. [21] Buhler, P., 2022. doi: 10.1002/essoar.10512516.1